J. Iron Steel Res. Int. (2024) 31:1936–1946
https://doi.org/10.1007/s42243-024-01176-8

ORIGINAL PAPER

Viscosity and structure of $CaO–BaO–SiO_2–Al_2O_3$-based mold slags for continuous casting of high titanium steel with different TiO_2 absorption

Ya-tao Cui[1] · Xue-you Wang[1] · Xu-bin Zhang[1] · Qiang-qiang Wang[1] · Sheng-ping He[1]

Received: 24 June 2023 / Revised: 9 August 2023 / Accepted: 8 September 2023 / Published online: 14 March 2024

Abstract
The effect of TiO_2 absorption into two different $CaO–BaO–SiO_2–Al_2O_3$-based mold slags from the steel plant on the viscosity, melting performance and microstructure of slags was investigated through the measurement of the viscosity–temperature relationship, melting temperature and Raman spectroscopy. The parameter of the number of non-bridging oxygen per tetrahedrally-coordinated atom (NBO/T) was also calculated to explain the microstructure variation of molten slags with different TiO_2 absorption. The variation of the actual slag consumption and the depth of the liquid slag in mold was explained through the comparison of the viscosity and the melting temperature of two different slags. The viscosity of mold slags (basicity = 0.6) decreased from 1.1 to 0.68 Pa s with the increase in the TiO_2 absorption from 0 to 10%, while that of slags (basicity = 0.7) decreased from 0.76 to 0.56 Pa s with the TiO_2 absorption from 0 to 6%. The activation energy of both two groups of slags had the tendency to decrease with the increasing TiO_2 absorption. The network structure of both two groups of slags measured by the Raman spectra showed that the fraction of complex structure units (Q^1, Q^2, Q^3 and Al–O–Al) decreased and simple structure units ($Al–O^-$ and Q^0) increased with the increase in TiO_2 absorption. NBO/T also increased with the increase in the TiO_2 absorption, indicating that the absorption of TiO_2 into slags resulted in the destruction of silicate/aluminate structure. Hence, the absorption of TiO_2 into the current $CaO–BaO–SiO_2–Al_2O_3$ mold slags decreased the degree of polymerization of these slags and then led to the decrease of viscosity.

Keywords Mold slag · Viscosity · Melting temperature · Slag consumption · Liquid slag depth · Structure

1 Introduction

High-Ti steel is gaining popularity with high strength, toughness, wear resistance, and ease of welding, among other qualities [1]. In the continuous casting of high-Ti steel, the TiO_x inclusion formed in the liquid steel could float up into the mold slag, and the steel–slag reaction also occurred [2–5], which caused the variation of the slag property, such as the melting performance, viscosity and crystallization, and then deteriorated the lubrication on the solidified shell and the heat transfer from the steel to the mold. During the casting of high-titanium steel (0.2% Ti), the TiO_2 content in slags increased from 0 (original slag) to approximately 6% (liquid slag), which directly affected the slag consumption and the surface quality of the billet (oscillation marks, depression, etc.). The increase in TiO_2 content in mold slags for a continuous casting of titanium-stabilized ferritic stainless steel was 3%–4% and the increase was roughly 6% for a titanium stabilized austenitic stainless steel [6]. Hence, it is necessary to understand the effect of TiO_2 content on the fundamental performance of mold slags.

For these years, many studies have been conducted to investigate the variation of slag properties with different TiO_2 contents, especially focused on the study of the blast furnace (BF) slag, and the fluorine-free mold slag. The effect of TiO_2 and basicity on viscosity of $CaO–SiO_2–7\%MgO–TiO_2–12\%Al_2O_3$ BF slags (CaO/SiO_2 = 0.5–0.9, TiO_2 = 15%–30%) was investigated by Liao et al. [7], and it was found that the slag viscosity decreased with

✉ Xu-bin Zhang
zhangxubin12@163.com

[1] College of Materials Science and Engineering, Chongqing University, Chongqing 400044, China

increasing both TiO_2 content and basicity. The effect of TiO_2 contents on viscosity and structure in CaO–SiO_2–17%Al_2O_3–10%MgO-based BF slags was investigated by Park et al. [8], and it was found that the TiO_2 content in slags from 0 to 10% resulted in the decrease of the slag viscosity through the depolymerization of the silicate network. A fluorine-free CaO–Al_2O_3–TiO_2 slag system was designed to reduce the slag-reaction by Piao et al. [9, 10] and it was found that low TiO_2 content (4%–8%) led to the increase in the viscosity, but excessive TiO_2 content (12%–16%) would be helpful to the decrease of the viscosity. The effect of TiO_2 content on structure characteristics in CaO–SiO_2–Al_2O_3-based fluorine-free mold slags (CaO/SiO_2 = 1) was studied [11], and it was found that the ratio of Q^2 structure units decreased and Q^0 structure units increased with TiO_2 content increasing from 0 to 10%, indicating that TiO_2 can destroy Si–O–Si network structure and some other complex structure groups. The influence of TiO_2 on viscosity and structure of CaO–Al_2O_3-based mold slags was studied by Li et al. [12], and it was found that viscosity of slags decreased gradually with TiO_2 content increasing from 0 to 10%, and the degree of polymerization of slags decreased with TiO_2 addition by destroying the Al–O complex structure groups. However, the influence of titanic oxide in high-titanium steel absorbed into the CaO–BaO–SiO_2–Al_2O_3-based mold slags with low fluorine and low basicity on the viscosity, melting temperature and microstructure of slags, and the corresponding depth of the liquid slag above the steel and slag consumption was not well discussed.

In the current study, the influence of different TiO_2 absorption into two actual CaO–BaO–SiO_2–Al_2O_3-based mold slags (BaO = 4%, F^- = 3.5%) from steel plant on the slag performance and structure was investigated. The viscosity–temperature relationship and melting temperature of two groups of slags with different TiO_2 contents were measured, and the depth of the liquid slag and the slag consumption of two original slags during the casting of high-Ti steel were compared. The activation energy of viscous flow and the microstructure through the Raman spectra and the parameter non-bridging oxygen per tetrahedrally-coordinated atom (NBO/T) were obtained to explain the variation of the slag viscosity.

2 Experimental methods

2.1 Sample preparation

In the current study, the properties of two mold slags used for the continuous casting of the same high-Ti steel in a steel plant were discussed. The Ti content of the steel was 0.2%, and the cross section of the mold and casting speed were 180 mm × 240 mm and 0.9 m/min, respectively. In order to understand the effect of TiO_2 in the molten steel floating into slags on the viscosity and structural characteristics, mold slags were designed with varying TiO_2 additions of 0, 2%, 4%, 6%, 8% and 10% into slags as group A (basicity = 0.6) and 0, 2%, 4% and 6% into slags as group B (basicity = 0.7), respectively. The mold slag from the steel plant was firstly decarburized in the air at 973 K, and then the mass of TiO_2 added into slag was calculated. The decarburized mold slag and the chemical of TiO_2 were mixed, and then pre-melted for 30 min in a $MoSi_2$ furnace at 1573 K to homogenize chemical compositions of slags. Subsequently, the molten slag was poured into a stainless crucible and cooled in the air to obtain homogeneous solid slag. X-ray fluorescence (XRF) spectroscopy was used to measure chemical compositions of pre-melted samples listed in Table 1. From Table 1, with the decomposition of a small amount of carbonate in the original mold slag, the percentage of TiO_2 in these premelted slags (Group A) was within 0.39%–11.43%. The content of F^- decreased from 3.48% to 0.78% with the increase in TiO_2 in slags, which was affected by the evaporation of fluorine. The evaporation ratio of fluoride was promoted with the increase in TiO_2 content in slags, proposed by Ju et al. [13], which explained the decrease of the fluorine content. The whole chemical composition of the mold slag (B1) without TiO_2 addition and only the TiO_2 content of slags (B2–B4) were measured. The percentage of the TiO_2 in these slags was within 0.34%–6.99%. The depth of the liquid slag and the slag consumption during the casting of the high-Ti steel with the use of original slags (A1 and B1) are also shown in Table 1, and these parameters of these two slags used in one of six-strand caster were measured under the same casting condition, respectively.

2.2 Viscosity measurement

In the current study, the viscosity–temperature relationship of mold slags in Table 1 was measured with the rotating cylinder method, and the schematic of the viscometer is shown in Fig. 1 [14]. Before viscosity measurement, the calibration of the temperature in the furnace and the viscosity of the fluid was conducted by the thermocouple and the standard oil [15], respectively. About 230 g molten slag was kept in the graphite crucible for 30 min when the temperature reached 1573 K to guarantee that the slag was totally melted and uniform. Afterward, the viscosity of the mold slag was continuously measured with the decrease of the slag temperature by 6 K/min, and then, the viscosity–temperature relationship of mold slags was obtained.

Table 1 Chemical compositions of mold slags and details of slags in service

Slag	No.	CaO/SiO_2	Al_2O_3/%	TiO_2/%	F^-/%	Na_2O/%	BaO/%	MgO/%	TiO_2 addition/%	Depth of liquid slag/mm	Slag consumption/(kg t^{-1})
Group A	A1	0.6	8.00	0.39	3.48	6.85	3.43	3.07	0	7–8	0.39
	A2	0.6	7.22	2.44	3.55	6.64	4.47	3.03	2	–	–
	A3	0.6	7.30	4.77	2.18	6.63	4.13	3.06	4	–	–
	A4	0.6	7.20	6.87	1.53	6.54	4.24	3.00	6	–	–
	A5	0.6	7.05	9.15	0.92	6.44	4.66	2.87	8	–	–
	A6	0.6	6.89	11.43	0.78	6.20	3.81	2.76	10	–	–
Group B	B1	0.7	6.89	0.34	3.58	6.72	3.14	3.18	0	6–7	0.45
	B2	0.7	–	2.83	–	–	–	–	2	–	–
	B3	0.7	–	4.64	–	–	–	–	4	–	–
	B4	0.7	–	6.99	–	–	–	–	6	–	–

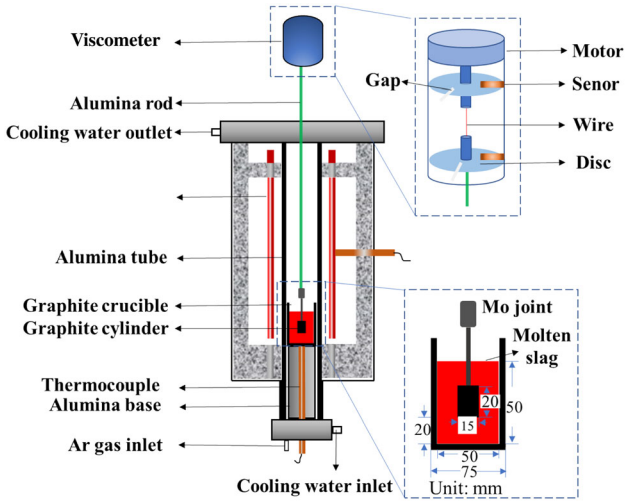

Fig. 1 Schematic of experimental setup for viscosity measurement [14]

2.3 Measurement of melting temperature

The hemisphere point method (CQKJ-II-type slag melting temperature characteristic tester) was used to measure the melting temperature of mold slags, and the schematic of the measurement equipment is shown in Fig. 2. The powder of the pre-melted slag was crushed into a cylindrical sample with the diameter of 3 mm and the length of 3 mm, and then placed in the tube furnace with the temperature increment at a speed of 25 K/min. The melting temperature of mold slag was obtained when the height of the cylindrical sample reached half of the initial one.

2.4 Structure analysis

In order to explain the performance changes of mold slags with different TiO_2 additions in slags, Raman spectrometry was used to obtain the structural characteristics of mold slags, which should be amorphous. During the sample preparation, the pre-melted slag was heated to 1573 K in the $MoSi_2$ furnace for 30 min to obtain homogeneous molten slag, and then partly quenched by water to form the glassy sample. The rest of the molten slag was poured into a container of iron material, and gradually cooled at the room temperature. Afterward, these slags quenched by water and cooled in the container were measured by the X-ray diffraction (XRD) method, as shown in Fig. 3 and all of the water-quenched samples and those cooled in the container were amorphous. Raman spectroscopy was conducted to study the microstructure of all water-quenched samples, and the spectra in the range of 200–1600 cm^{-1} was recorded. Finally, the scattering data were fitted using the Gaussian function through the Peakfit software.

3 Slag properties with different TiO_2 additions

3.1 Melting properties and viscosity

In the continuous casting of steel, the depth of the liquid slag pool, the thickness of slag film in the gap between the mold and solidified shell, and the slag consumption were largely influenced by melting properties and viscosity of mold slags. The melting temperature of two groups of slags is compared in Fig. 4a. With the increase in the TiO_2 addition from 0 to 10%, the melting temperature of mold slags (basicity = 0.6) decreased from 1439 to 1402 K, and the temperature increment is maintained at about 8 K with the same 2% TiO_2 addition. According to the slag composition in Table 1, the F^- content slightly decreased with the increase in TiO_2 addition, and the decrease of F^- in slags would result in the increase in the viscosity and

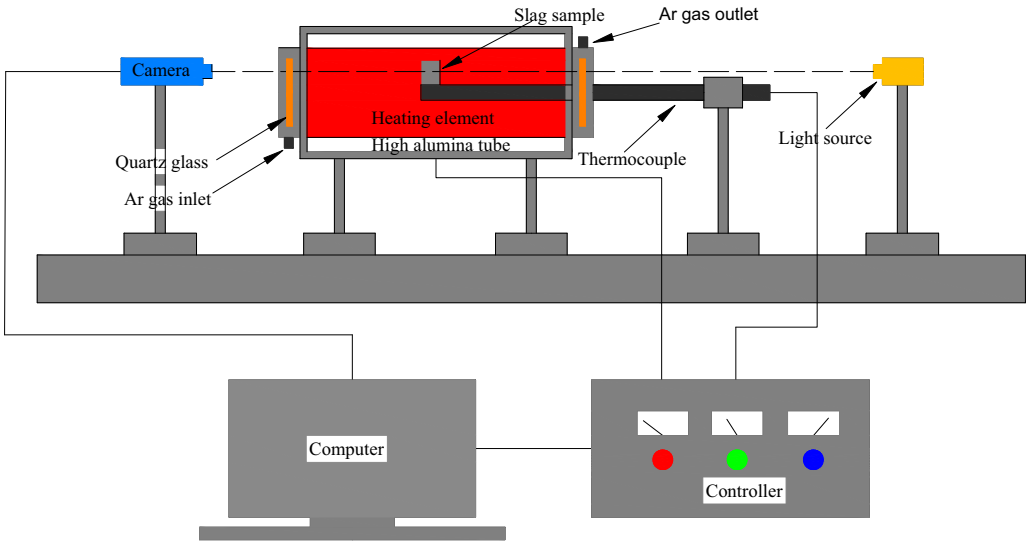

Fig. 2 Schematic of experimental setup for melting temperature measurement

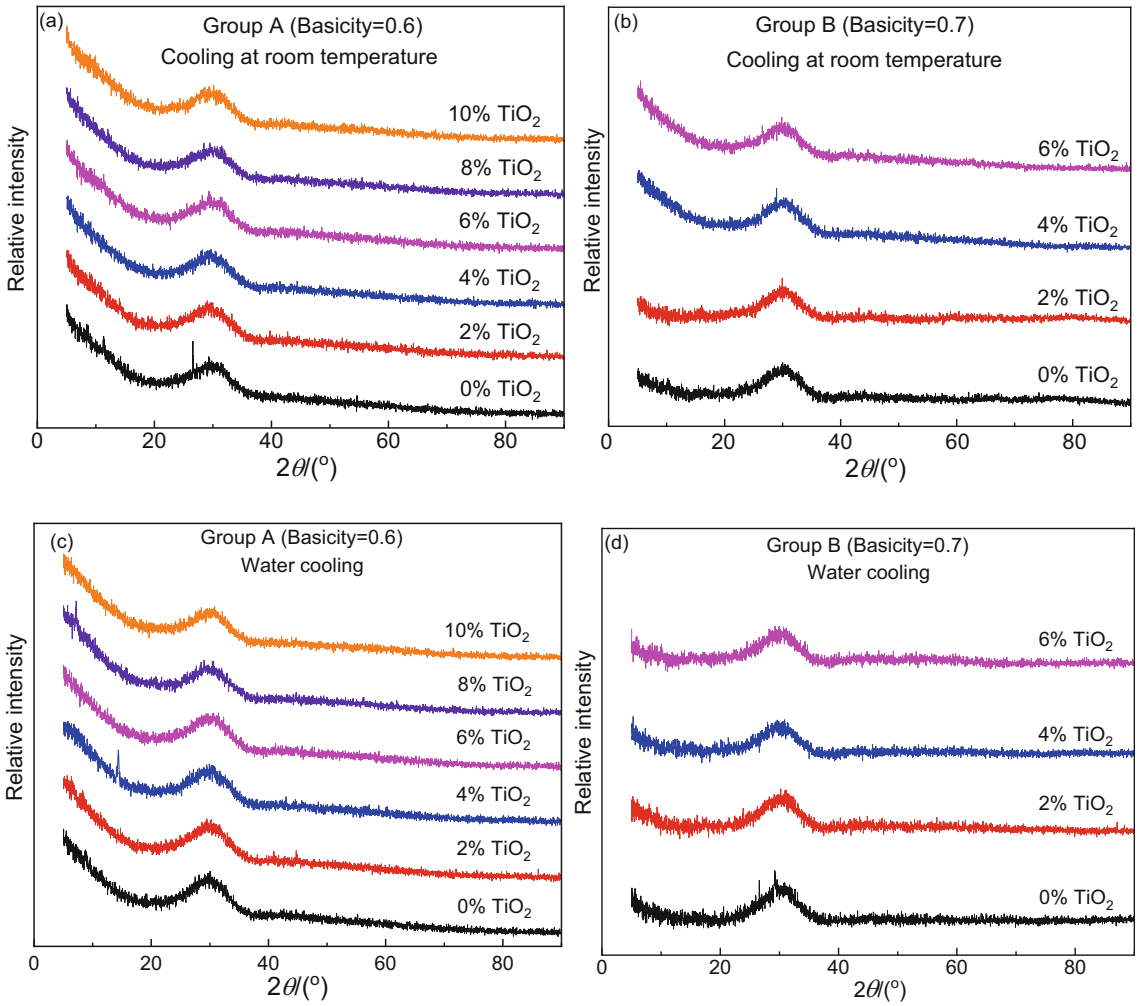

Fig. 3 XRD results of these slags with cooling at room temperature (**a**, **b**) and water cooling (**c**, **d**). 2θ—Diffraction angle

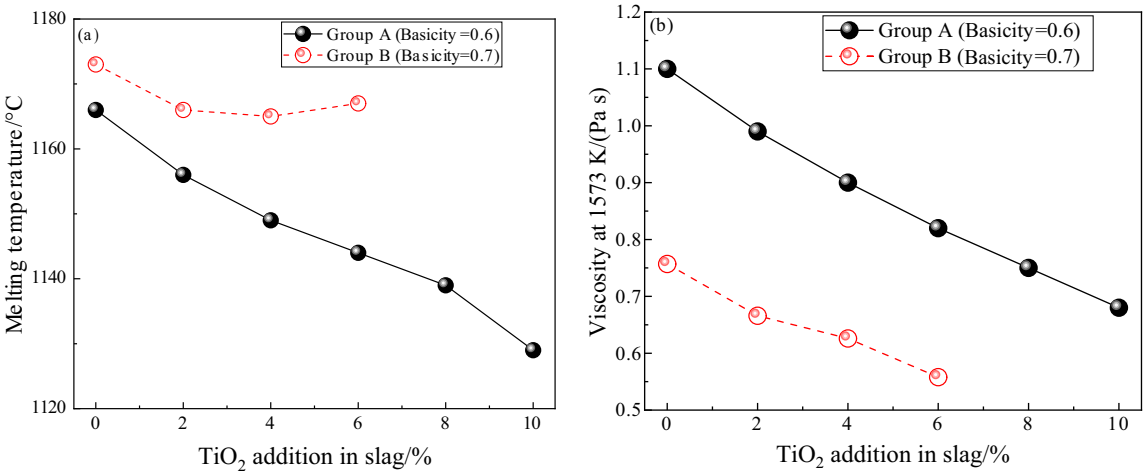

Fig. 4 Melting temperature (**a**) and viscosity at 1573 K (**b**) of mold slags with different TiO_2 additions

melting temperature of the slag, which was opposite to results in Fig. 4. Hence, the variation of the F^- content in slags was obviously smaller than that of TiO_2, and the variation of slag properties was determined by the difference of TiO_2 additions in slags. The melting temperature of slags (basicity = 0.7) slightly decreased from 1446 to 1439 K with the increase in the TiO_2 addition from 0 to 2% and then changed less (within 1438–1440 K) with the TiO_2 addition from 2% to 6%. Obviously, the melting temperature of slags with the basicity of 0.6 (group A) was lower than that of 0.7 (group B), resulting in the slight increase in the depth of the liquid slag pool in the mold, as shown in Table 1.

The viscosity of mold slags at 1573 K is compared with different TiO_2 additions of two groups of slags in Fig. 4b. The viscosity of slags in group A (basicity = 0.6) decreased from 1.1 to 0.68 Pa s, while that of slags in group B (basicity = 0.7) decreased from 0.76 to 0.56 Pa s with the increase in TiO_2 addition from 0 to 10% and 6%, respectively. The viscosity of slags at 1573 K had linear relationship with the addition of TiO_2 in slags, and the variation of viscosity is approximately 0.042 Pa s (group A) and 0.033 Pa s (group B) with the same 1% TiO_2 addition, respectively. Obviously, the viscosity of slags at 1573 K with the basicity of 0.6 (group A) was larger than that of 0.7 (group B), resulting in the increase in the slag consumption with the same casting condition in a steel plant, as shown in Table 1. Hence, the increase in the TiO_2 content in the low-basicity slag through the floating of TiO_2 inclusions in the mold could lead to the decrease of slag viscosity.

Viscosity–temperature relationship measured during the cooling process (6 K/min) of two groups of slags with different TiO_2 addition is illustrated in Fig. 5. Viscosity of all mold slags (groups A and B) gradually increased with the decrease of the slag temperature, and no apparent break points were obtained along the viscosity–temperature curve, indicating that these two low-basicity mold slags still existed as acid slags (or long slags) after the absorption of 0–10% TiO_2, and had weak crystallization ability without break points or conspicuous crystal precipitation in slags with the decrease of the temperature [15]. Besides, the TiO_2 addition into slags from 0 to 10% or 6% had relatively small influence on the crystallization property of slags, which could also be demonstrated by XRD results of amorphous slags obtained through the slow cooling in the room temperature, as shown in Fig. 3a, b. Certainly, the viscosity–temperature relationship and the XRD results could only qualitatively indicate the crystallization ability of slags [16], and the crystallization rate, initial crystallization temperature and crystallization kinetics analysis should be conducted to obtain the accurate comparison of slag crystallization, which would be discussed in following studies.

3.2 Activation energy of viscous flow

The activation energy of the viscous flow represents the frictional resistance within the structural units of the melt that needs to be overcome during shearing or the flow of the slag [17]. Activation energy varied due to changes of microstructure, and that is expected to be constant before precipitation happens for a certain slag system. The relationship between $\ln\eta$ and $1/(RT)$ (where η is the viscosity of mold slags, Pa s; R is the gas constant, 8.314 kJ/mol; and T is the absolute temperature, K) with different TiO_2 additions was calculated through the Arrhenius equation (Eq. (1)), and the linear fitting results of two groups of slags are shown in Fig. 6 to understand the effect of TiO_2 addition on the activation energy of these molten slags.

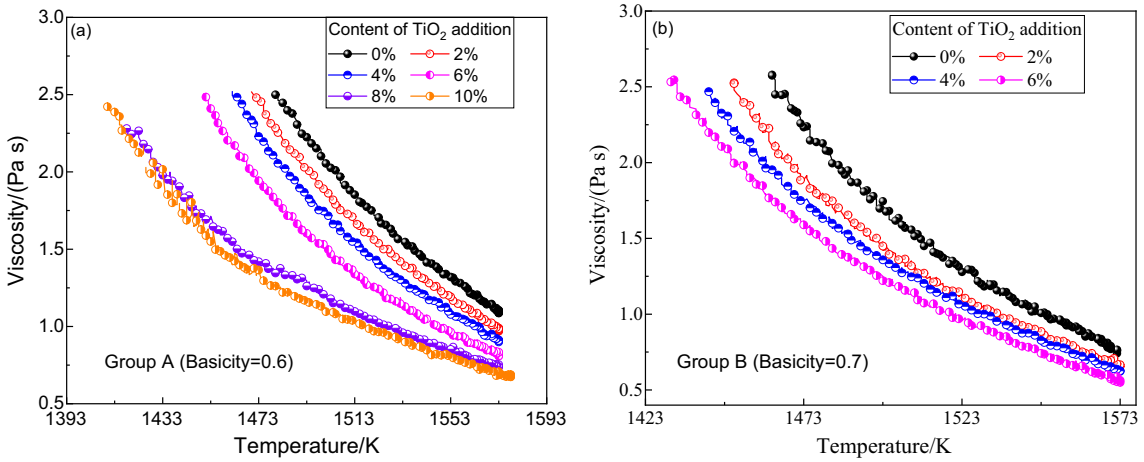

Fig. 5 Viscosity–temperature curves of mold slags with different TiO_2 additions in slags of group A (**a**) and group B (**b**)

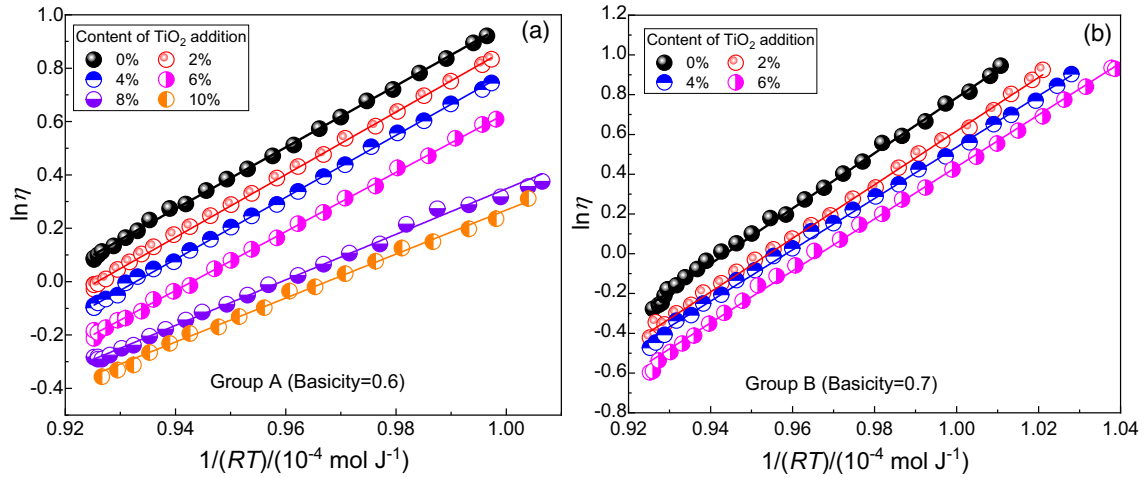

Fig. 6 Fitting curves of $\ln\eta$ *vs.* $1/(RT)$ for slags of group A (**a**) and group B (**b**)

From Fig. 6, only one fitting line was obtained, and the slope of the fitting line was compared as the activation energy of the viscous flow with different TiO_2 additions in slags, as shown in Fig. 7. The activation energy of viscous flow decreased in both groups of slags with the increase in TiO_2 addition, indicating that the energy barrier for the flowing of the molten slag was reduced and the microstructure of the melt became simple. Particularly, the activation energy marginally decreased with the increase in TiO_2 addition from 0 to 6% in both groups, but the variation increased with the TiO_2 addition from 6% to 8% of mold slags in group A, indicating that the microstructure of the melt became simple, and the influence of the temperature (or the thermal motion of molecule) on the viscosity of the molten slag decreased.

$$\ln\eta = \ln\eta_0 + \frac{E_n}{RT} \tag{1}$$

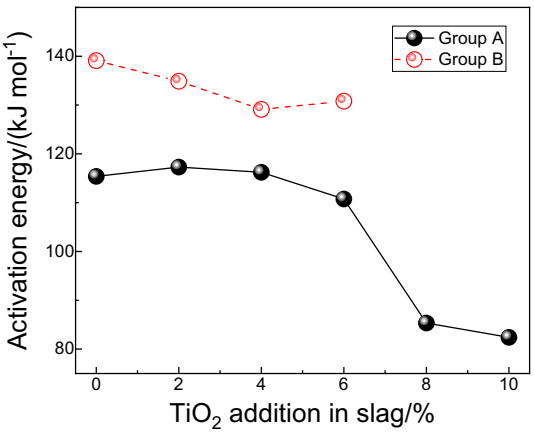

Fig. 7 Calculated activation energy of viscous flow for slag samples

where η_0 is the pre-exponential factor, Pa s; and E_η is the viscous flow activation energy of the slag, kJ/mol.

4 Effect of TiO_2 addition on structure of mold slags

4.1 Structure through Raman spectra

In order to understand the variation of slag microstructure with different TiO_2 additions into slags, the Raman spectra of water-quenched glassy samples was measured, as shown in Fig. 8. From Fig. 8, the spectral curve was divided into two regions, the high frequency region between 800 and 1100 cm^{-1} and low frequency region between 500 and 800 cm^{-1}. Only one peak centered at ~ 560 cm^{-1} appeared in the low-frequency region, while two peaks were located at 910 and 1025 cm^{-1} in the high-frequency region. In the low-frequency region, the peak around 560 cm^{-1} had no obvious change in intensity with the increase in TiO_2 addition. In the high-frequency region, the peak around 910 cm^{-1} remained with high intensity and great width, shifting from ~ 910 to 875 cm^{-1}, whereas the peak at 1025 cm^{-1} became low.

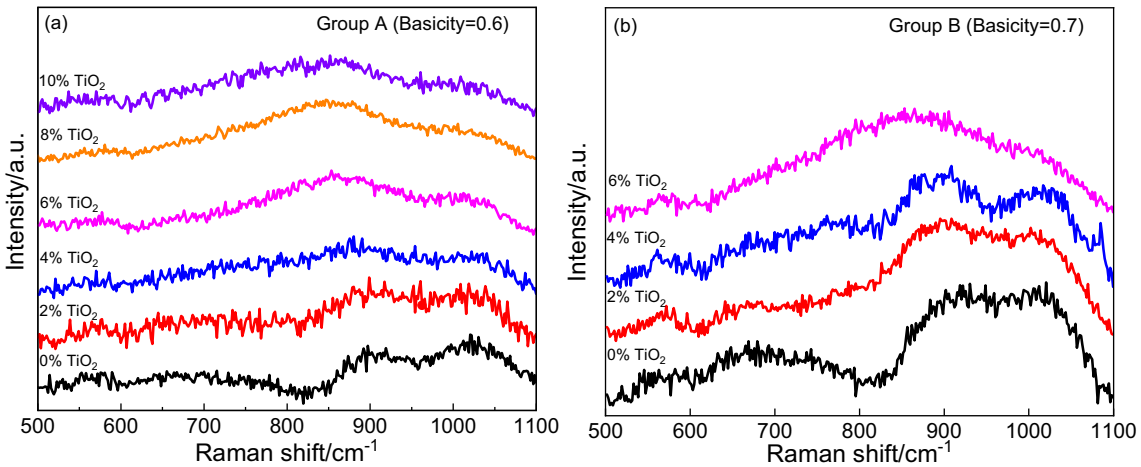

Fig. 8 Raman spectral curves of quenched samples of group A (**a**) and group B (**b**)

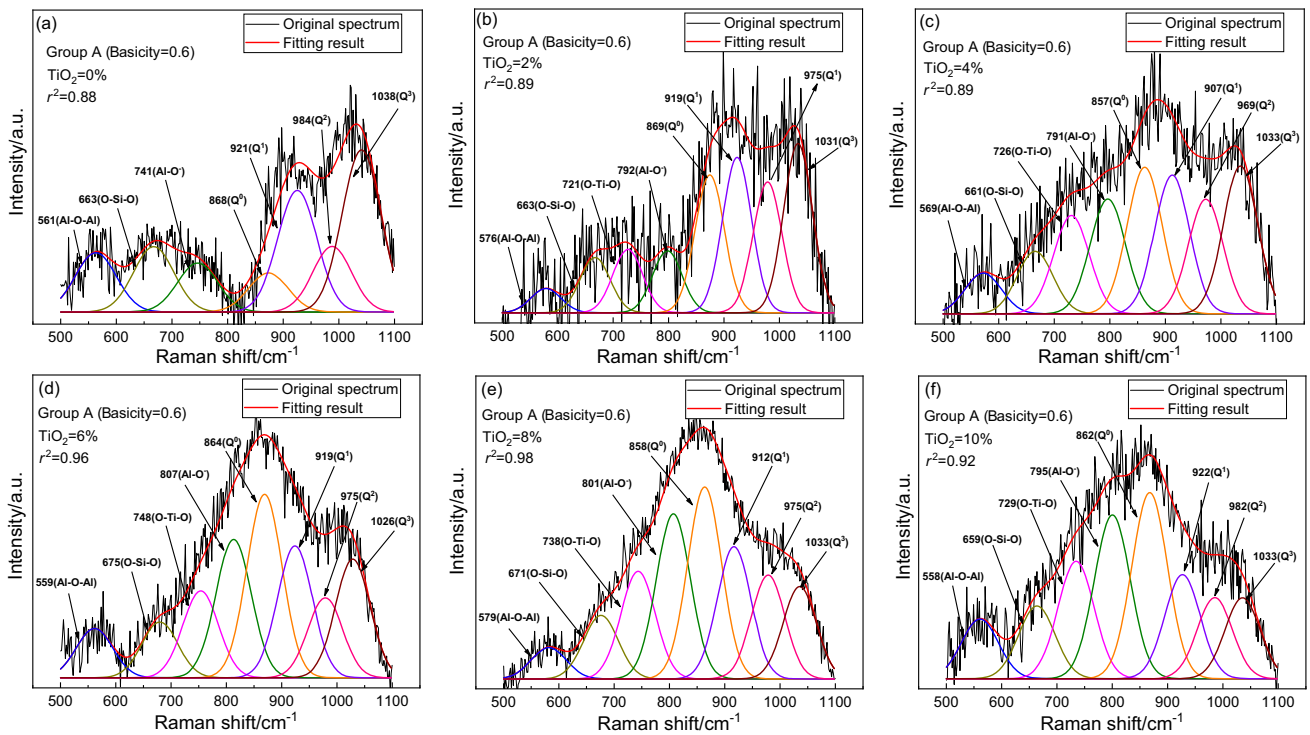

Fig. 9 Deconvoluted results of Raman spectral curves for glassy samples of group A. r^2—Coefficient of determination

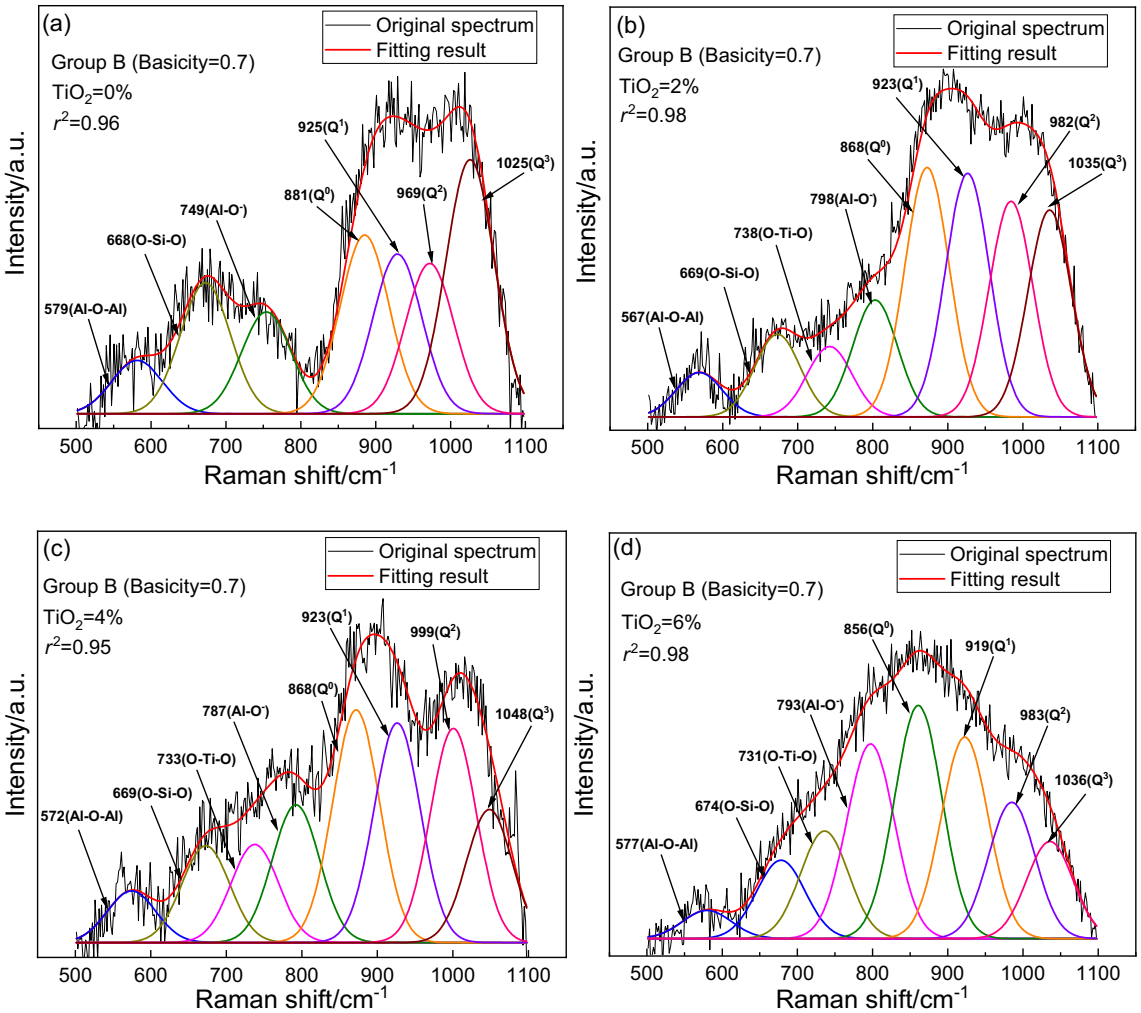

Fig. 10 Deconvoluted results of Raman spectral curves for glassy samples of group B

Raman curves for the analysis of the slag structure were deconvoluted using the Gaussian-Deconvolution method, as shown in Figs. 9 and 10 the recommended frequency of Raman bands is summarized in Table 2. The deconvoluted bands in the low-frequency region were assigned to the aluminate group, with the peak around 550 cm^{-1} attributed to the Al–O–Al linkage, which was the major bond in the 3D aluminate network. The band with the frequency of about 659–676 cm^{-1} could be relevant to the deformation motion of O–Si–O, peaks centered around 722 to 738 cm^{-1} in Ti-bearing samples were probably assigned to deformation of O–Ti–O or O–(Si, Ti)–O in chain or sheet units or both, and those at around 770 cm^{-1} were related to Al–O^- stretching vibration in [AlO_4] units with one or two nonbridging oxygen (NBO). The Raman signal between 800 and 1100 cm^{-1} represented the symmetric stretching vibration of [SiO_4]-tetrahedra in silicate network, which was essential to study the structural units comprising silicate-dominant slag systems. These [SiO_4]-tetrahedra units with peaks in the ranges of 850–880, 900–930, 950–980, and 1010–1040 cm^{-1} could be ascribed to the stretching vibrations of the Si–O bonds in Q^0 (NBO/Si = 4, [SiO_4]-monomer), Q^1 (NBO/Si = 3, [Si_2O_7]-dimer), Q^2 (NBO/Si = 2, [SiO_3]-chain), and Q^3 (NBO/Si = 1, [Si_2O_5]-sheet),

Table 2 Structure assignments of Raman bands in spectra of mold slags

Raman shift/cm^{-1}	Raman assignment	Reference
~ 550	Al–O–Al	[12, 18–21]
659–676	O–Si–O	[22, 23]
722–738	O–Ti–O or O–(Si, Ti)–O	[24, 25]
~ 770	Al–O^-	[26–29]
~ 860	Q^0	[30–33]
900–930	Q^1	[12, 30–32]
~ 960	Q^2	[33, 34]
~ 1050	Q^3	[35–37]

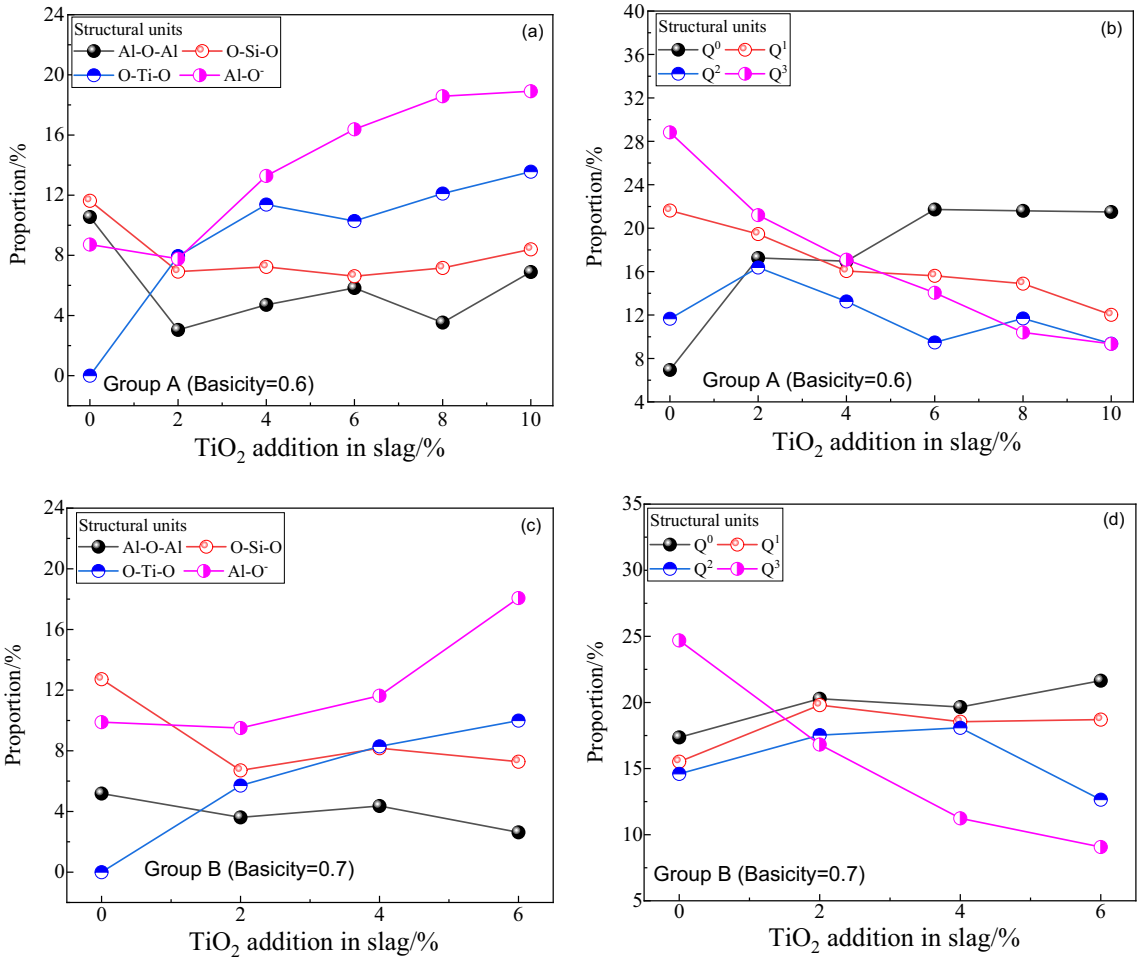

Fig. 11 Proportions of structure units of simple units (**a**, **c**) and Q^0–Q^3 (**b**, **d**) obtained from deconvolution of Raman spectra. **a**, **b** Group A; **c**, **d** group B

respectively, and n in the Q^n structural units indicated the number of bridging oxygen atoms per silicate atom.

The proportion of each unit is shown in Fig. 11, which is calculated as the ratio of the covered area below the corresponding curve and the total area below all these curves in Figs. 9 and 10. The proportion of the structural unit Q^3 decreased from 28.8% to 9.3% and that of Q^0 increased from 6.9% to 21.5% in group A (basicity = 0.6) with the increase in the TiO_2 addition from 0 to 10%. The proportion of structural unit Q^3 decreased from 24.7% to 9.1% and that of Q^0 increased from 17.4% to 21.6% in group B (basicity = 0.7) with the increase in the TiO_2 addition from 0 to 6%, indicating the decrease of the degree of polymerization and the complexity in silicate network structure of molten slags. The proportion of unit Al–O–Al had the decreasing trend with the increase in TiO_2 addition. The proportion of the structural unit O–Ti–O or O–(Si, Ti)–O increased from 0 to 13.6%, and that of Al–O^- increased from 8.7% to 18.9% in group A (basicity = 0.6) with the TiO_2 addition from 0 to 10%. The proportion of the structural unit O–(Si, Ti)–O increased from 0 to 9.9%, and that of Al–O^- increased from 9.9% to 18.7% in group B (basicity = 0.7) with the TiO_2 addition from 0 to 6%, which indicated that aluminate structure became simple through Al–O–Al structural unit transformation into Al–O^- structural unit and some [TiO_4] were incorporate into silicate network to form O–(Si, Ti)–O [38]. Hence, the increase in TiO_2 addition caused the breakage of both silicate and aluminate network structure, ultimately resulting in the decrease of the polymerization degree of molten slags and also the decrease of the slag viscosity in Fig. 4.

4.2 Structure through parameter NBO/T

Usually, NBO/T is used to represent the degree of polymerization of the melt [39]. The ratio of NBO/T is related to the complexity of the overall structure, and the decrease of NBO/T is an indication of depolymerization occurring

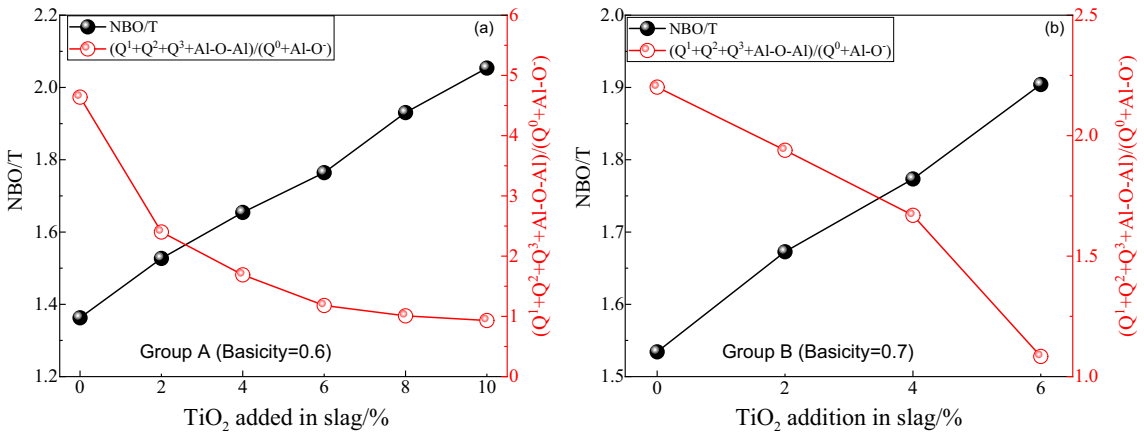

Fig. 12 Comparison among percentage ratio of (Q^1 + Q^2 + Q^3 + Al–O–Al)/(Q^0 + Al–O^-) and parameter NBO/T. **a** Group A; **b** group B

within the structure of the molten slag. Additionally, the composition of CaF_2 is usually not considered when the NBO/T is calculated [40, 41], and the content of F^- is low (below 3.0%). The modified calculation equation of NBO/T is shown as follows:

$$\mathrm{NBO/T}=\frac{2\left(x_{\mathrm{CaO}}+x_{\mathrm{Na_2O}}+2x_{\mathrm{TiO_2}}+x_{\mathrm{BaO}}+x_{\mathrm{MgO}}\right)-2x_{\mathrm{Al_2O_3}}}{x_{\mathrm{SiO_2}}+2x_{\mathrm{Al_2O_3}}} \quad (2)$$

where x is the mole fraction of each component in slags.

In Fig. 12, the parameter NBO/T of molten slags with different TiO_2 additions is shown, and NBO/T and the ratio of complex structure units (Q^1, Q^2, Q^3, and Al–O–Al) and simple structure units (Q^0 and Al–O^-) are compared. The parameter NBO/T gradually increased from 1.36 to 2.05 with the increase in TiO_2 addition from 0 to 10% in group A, and that also gradually increased from 1.53 to 1.90 with the increase in TiO_2 addition from 0 to 6% in group B. The ratio of complex structure units (Q^1, Q^2, Q^3, and Al–O–Al) and simple structure units (Q^0 and Al–O^-) decreased with increase in TiO_2 addition in both groups of slags, indicating that complex structural units gradually transformed into simple structural units and the number of non-bridging oxygen increased. From Fig. 12, the variation of the percentage ratio between complex structure units and simple structure units had negative correlation with NBO/T and had positive correlation with that of the viscosity of molten slags in Fig. 5, indicating that the decrease in slag viscosity is related to the depolymerization of slag structure. With the increase in simple structure units and decrease of complex structure units in molten slags, the degree of polymerization or complexity of slags decreased, which resulted in the easy movement of structural units in slags and low viscosity of molten slags [23, 42]. Hence, the TiO_2 in current mold slags primarily behaved as a basic oxide by supplying free oxygen ions (O^{2-}), and the increase in the TiO_2 addition into slags caused the decrease of the polymerization degree of mold slags and then resulted in the decrease of the viscosity of these current CaO–BaO–SiO_2–Al_2O_3-based slags as well as the increase in the slag consumption in the continuous casting of high-Ti steel in Table 1.

5 Conclusions

1. With the addition of the TiO_2 into current slags from 0 to 10%, the viscosity at 1573 K of mold slags (basicity = 0.6) decreased from 1.1 to 0.68 Pa s and that of slags (basicity = 0.7) decreased from 0.76 to 0.56 Pa s. The melting temperature of slags (basicity = 0.6) decreased from 1439 to 1402 K and that of slags (basicity = 0.7) decreased from 1446 to 1439 K. With basicity of the slag from 0.6 to 0.7, the slag viscosity decreased, but the melting temperature increased, resulting in the increase in slag consumption and the decrease of the depth of the liquid slag.
2. According to results by the Raman spectra method and the parameter NBO/T, with the increase in TiO_2 addition into the acid slag from 0 to 10%, complex structure units were transformed into simple structure units and the number of non-bridging oxygen increased, which simplified the network structure. Then, the degree of polymerization of the mold slags decreased and closely correlated to the decrease of the slag viscosity.

Acknowledgements The authors are grateful for support from the National Natural Science Foundation China (Grant Nos. 52274317, 52074054, and 52004045), the Fundamental Research Funds for the Central Universities (Grant No. 2023CDJXY-020), and College of Materials Science and Engineering at Chongqing University, China, and the Henan Tongyu Metallurgy Materials Group Co. Ltd., Xixia, China.

Declarations

Conflict of interest All authors declare that there are no competing interests.

References

[1] X.J. Wang, S. Qu, R. Liu, L.G. Zhu, Z.L. Piao, T.C. Di, Y. Wang, Mater. Rep. 35 (2021) No. Z1, 467–472.
[2] Z. Hao, W. Chen, C. Lippold, Metall. Mater. Trans. B 41 (2010) 805–812.
[3] Z. Wang, Q.F. Shu, X.M. Hou, K.C. Chou, Ironmak. Steelmak. 39 (2012) 210–215.
[4] L. Zhou, Z. Pan, W. Wang, J. Chen, L. Xue, T. Zhang, L. Zhang, Metall. Mater. Trans. B 51 (2020) 85–94.
[5] Z. Wang, Q. Shu, K. Chou, Metall. Mater. Trans. B 44 (2013) 606–613.
[6] T. Mukongo, P.C. Pistorius, A.M. Garbers-Craig, Ironmak. Steelmak. 31 (2004) 135–143.
[7] J.L. Liao, J. Li, X.D. Wang, Z.T. Zhang, Ironmak. Steelmak. 39 (2012) 133–139.
[8] H. Park, J.Y. Park, G.H. Kim, I. Sohn, Steel Res. Int. 83 (2012) 150–156.
[9] Z. Piao, L. Zhu, X. Wang, Z. Liu, B. Wang, P. Xiao, Z. Yuan, Metall. Mater. Trans. B 51 (2020) 2119–2130.
[10] Z. Piao, Research on exploitation and metallurgical properties of CaO-Al_2O_3-TiO_2-based mold flux for high titanium steel, University of Science and Technology Beijing, Beijing, China, 2021.
[11] Z. Wang, Q. Shu, K. Chou, High Temp. Mater. Process. 32 (2013) 265–273.
[12] J.L. Li, Q.F. Shu, K.C. Chou, Can. Metall. Quart. 54 (2015) 85–91.
[13] J.T. Ju, G.H. Ji, J.L. An, C.M. Tang, Ironmak. Steelmak. 48 (2021) 109–115.
[14] Z. Li, Research on reactivity control and basic structure properties of mold flux for high-Mn high-Al steel, Chongqing University, Chongqing, China, 2019.
[15] L. Zhu, Q. Wang, Q. Wang, S. Zhang, S. He, Ironmak. Steelmak. 46 (2019) 865–871.
[16] L.L. Zhu, Q. Wang, Q.Q. Wang, S.D. Zhang, Ironmak. Steelmak. 46 (2019) 865–871.
[17] G. Urbain, Y. Bottinga, P. Richet, Geochim. Cosmochim. Acta 46 (1982) 1061–1072.
[18] P. McMillan, B. Piriou, A. Navrotsky, Geochim. Cosmochim. Acta 46 (1982) 2021–2037.
[19] E. Gao, W. Wang, L. Zhang, J. Non-Cryst. Solids 473 (2017) 79–86.
[20] Y. Sun, H. Wang, Z. Zhang, Metall. Mater. Trans. B 49 (2018) 677–687.
[21] I. Daniel, P. Gillet, B.T. Poe, P.F. McMillan, Phys. Chem. Miner. 22 (1995) 74–86.
[22] B.O. Mysen, D. Virgo, C.M. Scarfe, Am. Mineralogist 65(1980) 690–710.
[23] D.L. Zheng, C.B. Shi, Z.J. Li, J. Li, J.W. Cho, J. Iron Steel Res. Int. 27 (2020) 33–41.
[24] B. Mysen, D. Neuville, Geochim. Cosmochim. Acta 59 (1995) 325–342.
[25] B. Mysen, F. Ryerson, D. Virgo. Am. Mineralogist 65 (1980) 1150–1165.
[26] Z. Yan, X. Lv, Z. Pang, X. Lv, C. Bai, Metall. Mater. Trans. B 49 (2018) 1322–1330.
[27] L. Zhou, H. Li, W. Wang, D. Xiao, L. Zhang, J. Yu, Metall. Mater. Trans. B 49 (2018) 2232–2240.
[28] D. Liang, Z. Yan, X. Lv, J. Zhang, C. Bai, Metall. Mater. Trans. B 48 (2017) 573–581.
[29] J. Ji, Y. Cui, S. Wang, S. He, Q. Wang, X. Zhang, Ceram. Int. 48 (2022) 256–265.
[30] Z.J. Wang, Q.F. Shu, S. Sridhar, M. Zhang, Metall. Mater. Trans. B 46 (2015) 758–765.
[31] B. Mysen, L. Finger, V. David, F. Seifert. Am. Mineralogist 67(1982) 686–695.
[32] B.O. Mysen, D. Virgo, F.A. Seifert, Rev. Geophys. 20 (1982) 353–383.
[33] L.G. Hwa, S.L. Hwang, L.C. Liu, J. Non-Cryst. Solids 238 (1998) 193–197.
[34] J. Li, Y. Sun, Z. Li, Z. Zhang, ISIJ Int. 56 (2016) 752–758.
[35] R. Akagi, N. Ohtori, N. Umesaki, J. Non-Cryst. Solids 293–295 (2001) 471–476.
[36] J. Tan, S. Zhao, W. Wang, G. Davies, X. Mo, Mater. Sci. Eng. B 106 (2004) 295–299.
[37] B. Mysen, J. Frantz, Contrib. Mineral. Petrol. 117 (1994) 1–14.
[38] Z. Wang, Q. Shu, K. Chou, ISIJ Int. 51 (2011) 1021–1027.
[39] K.C. Mills, ISIJ Int. 33 (1993) 148–155.
[40] X. Yan, W. Pan, X. Wang, X. Zhang, S. He, Q. Wang, Metall. Mater. Trans. B 52 (2021) 2526–2535.
[41] Y. Sasaki, M. Iguchi, M. Hino, ISIJ Int. 47 (2007) 638–642.
[42] D.L. Zheng, G.J. Ma, X. Zhang, M.K. Liu, J. Xu, J. Iron Steel Res. Int. 30 (2023) 717–725.